Kinetic Phase Diagram for Nucleation and Growth of Competing Crystal Polymorphs in Charged Colloids

Willem Gispen* and Marjolein Dijkstra†
Soft Condensed Matter, Debye Institute for Nanomaterials Science, Utrecht University, Utrecht 3584 CC, The Netherlands

(Received 14 March 2022; revised 27 May 2022; accepted 28 June 2022; published 26 August 2022)

We determine the kinetic phase diagram for nucleation and growth of crystal phases in a suspension of charged colloids. Exploiting the seeding approach in extensive simulations, we calculate nucleation barrier heights for face-centered cubic (fcc) and body-centered cubic (bcc) phases for varying screening lengths and supersaturations. We determine for the entire metastable fluid region the crystal polymorph with the lowest nucleation barrier, and find a regime close to the triple point where metastable bcc can form due to a lower nucleation barrier, even though fcc is the stable phase. For higher supersaturation, we find that the difference in barrier heights decreases and we observe a mix of hexagonal close-packed, fcc, and bcc structures in the growth of crystalline seeds as well as in spontaneously formed crystals. Our kinetic phase diagram rationalizes the different crystallization mechanisms observed in previous work.

DOI: 10.1103/PhysRevLett.129.098002

Crystallization plays a prominent role in many research areas and industrial processes, including weather prediction, protein characterization, and pharmaceutical drugs production. However, the kinetic pathways of nucleation and the mechanisms of polymorph selection during crystallization are far from being well-understood. For example, the end product of crystallization is not necessarily the stable structure and can even be an undesired phase. More complicated scenarios are also possible with structural transformations taking place at various stages of the crystallization process.

Colloidal suspensions are ideal for studying nucleation and crystallization as the particle coordinates can be tracked by advanced microscopy due to the relatively large size and slow diffusion of the colloids [1–3]. Charge-stabilized colloids are specifically suited for studying the selection between crystal polymorphs, since they show an intriguing competition between face-centered cubic (fcc) and body-centered cubic (bcc) crystal phases. However, the crystallization mechanism in charged colloids is not clear-cut and numerous experimental observations are hitherto unexplained. For instance, the observation of broad fluid-solid and fcc-bcc coexistences in various experiments [4,5] is inconsistent with the theoretical phase diagrams [6] that predict narrow phase coexistences. Furthermore, a wide variety of crystallization mechanisms has been observed in experiments, ranging from a simple one-step nucleation mechanism of fcc crystals [7,8] to the emergence of metastable bcc crystals that subsequently transform into fcc [9,10], as well as the emergence of hexagonal close-packed (hcp) before fcc is formed [11].

Simulations do not seem to reach consensus either, as they report conflicting results such as the observation of predominantly bcc-structured (pre)critical nuclei in regions where fcc is stable [12,13], a two-stage fluid-fcc crystallization via an intermediate bcc phase [14], formation of bcc-ordered precursors [15], or the formation of metastable bcc with numerous cross-nucleations of hcp on stable fcc and fcc on metastable hcp crystals [16]. It is important to note that simulations of crystallization are prohibitively slow because nucleation is a rare event. Hence, simulation studies on nucleation are limited to only a few state points and interaction parameters, making it difficult to obtain a coherent picture of the different nucleation mechanisms. Moreover, these simulations can only be performed at high supersaturations.

To date, we can only rely on simple guidelines to predict how a system crystallizes. In 1879, Ostwald formulated his famous step rule that the phase that nucleates need not be the stable phase, but may also be the phase that is closest in free energy to the metastable fluid phase, i.e., the less stable polymorph. This would result in a complete reversal of the thermodynamic phase diagram, i.e., fcc nucleates when bcc is stable and bcc forms when fcc is stable. In the 1930s, Stranski and Totomanov conjectured that the phase that nucleates should have the lowest free-energy barrier with the fluid phase, which can be different from the stable phase. Finally, Alexander and McTague argued on the basis of Landau theory and general symmetry considerations that nucleation of bcc is always favored at low supersaturations in the case of weakly first-order freezing transitions [17]. It is clear that these rules of thumb are too general to be universally valid. For example, both Ostwald's step rule and the Stranski-Totomanov conjecture were shown to be violated in a lattice model of patchy particles [18]. For charged colloids, at high screening close to the hard-sphere

limit, bcc is mechanically unstable thereby violating Alexander and McTague's conjecture.

In this Letter, we present a coherent picture of the different crystallization scenarios of charged colloids. We first determine the equilibrium phase diagram as a function of screening length and pressure using free-energy calculations. We then calculate the nucleation barrier heights for the full region of the phase diagram where fcc is the thermodynamically stable phase using extensive simulations based on the seeding technique [19]. The seeding approach allows us not only to determine nucleation barriers at relatively low supersaturation but also to compare the barrier heights of competing crystal structures. We then characterize the structure of growing crystals obtained from both seeded and brute-force simulations. In this way, we obtain a kinetic phase diagram containing information about the nucleation as well as the growth stages of crystallization.

We consider a charge-stabilized colloidal suspension, which is well-described by a system where the electrostatic interactions between the colloids are described by a screened Coulomb (Yukawa) potential,

$$\beta u_Y(r) = \beta\epsilon \frac{\exp[-\kappa\sigma(r/\sigma - 1)]}{r/\sigma},$$

with $\beta\epsilon$ the contact value and $1/\kappa\sigma$ the Debye screening length that determine the strength and range of the repulsion, respectively. The excluded-volume interactions between the colloids are represented by a pseudo-hard-core potential $\beta u_{\mathrm{PHS}}(r)$ that reproduces well the hard-sphere equation of state [20]. The total interaction potential of the pseudo-hard-core Yukawa system reads $\beta u(r) = \beta u_Y(r) + \beta u_{\mathrm{PHS}}(r)$. We set $\beta\epsilon = 81$ throughout this Letter. We note that for this high contact value the phase behavior of this pseudo-hard-core Yukawa system can be mapped onto that of point Yukawa particles as shown in Ref. [6]. Consequently, our results are valid for any contact value that is sufficiently high, i.e., $\beta\epsilon > 20$, by exploiting the mapping of point Yukawa particles onto hard-core Yukawa particles [6].

We determine the bulk equilibrium phase diagram for charged colloids with a contact value $\beta\epsilon = 81$ using free-energy calculations; see Supplemental Material (SM) [21] for technical details. We present the phase diagram in the reduced pressure $\beta P\sigma^3$-Debye screening length $1/\kappa\sigma$ representation in Fig. 1. The phase diagram displays fluid-fcc, fluid-bcc, and bcc-fcc binodals and their metastable extensions, denoted by solid and dotted lines, respectively, as well as a triple point at Debye screening length $1/\kappa\sigma \approx 0.22$ and pressure $\beta P\sigma^3 \approx 6.7$ in good agreement with Ref. [6]. Hence, the bcc phase is only stable for $1/\kappa\sigma \gtrsim 0.22$. In addition, we identify the stability regions of the fluid and the bcc phase, by determining at which pressure the fluid spontaneously crystallizes and the bcc spontaneously transforms into fcc. We denote the boundaries where fluid and bcc become unstable by a dash-dotted and dashed line, respectively. It is clear that at high screening the Alexander-McTague conjecture stating that nucleation of bcc should be favored near melting is violated as the bcc phase is simply unstable. Moreover, both the Alexander-McTague conjecture and Ostwald's step rule stating that the least stable polymorph should nucleate first cannot be valid in the region between the fluid-fcc binodal and the metastable fluid-bcc binodal as the bcc phase has a higher Gibbs free energy than the fluid phase; see also SM [21].

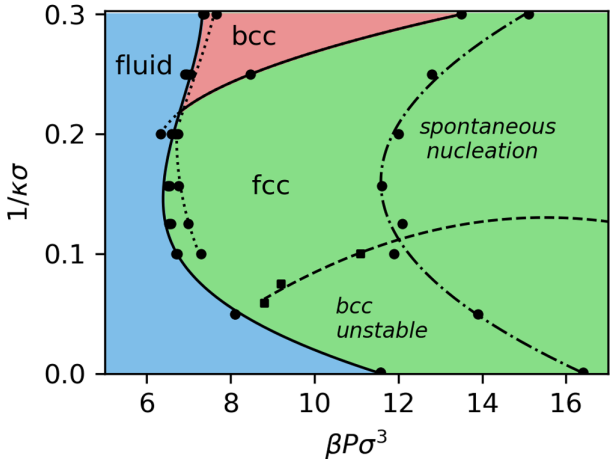

FIG. 1. Bulk phase diagram of highly charged colloids with a contact value $\beta\epsilon = 81$ in the pressure $\beta P\sigma^3$-Debye screening length $1/\kappa\sigma$ plane. The fluid-fcc, fluid-bcc, and bcc-fcc binodals are denoted by solid lines and their metastable extensions by dotted lines. The dash-dotted line marks the pressure at which the fluid spontaneously crystallizes. The dashed line indicates where the bcc phase spontaneously transforms into fcc. Dots are the actual measurements; lines are spline interpolations to guide the eye.

To study the kinetic competition between fcc and bcc crystal polymorphs, we use a method similar to recent work on metastable phases in iron [30]. Compared to Ref. [30], we build our method more explicitly on the seeding technique [19], which has been used and validated in many different systems over the past few years, e.g., in hard spheres [31], oppositely charged colloids [32], and NaCl [33]. The seeding technique allows us to efficiently measure the nucleation barriers for relatively low supersaturation, but more importantly to also compare directly the nucleation barriers of fcc and bcc. The method relies on the combination of molecular dynamics simulations with classical nucleation theory. According to that theory, the Gibbs free-energy barrier height ΔG^* is related to the supersaturation $|\Delta\mu| = |\mu_x - \mu_f|$, i.e., the difference in chemical potential between the stable crystal μ_x and supersaturated fluid phase μ_f as

$$\Delta G^* = \frac{1}{2} N^* |\Delta\mu|, \tag{1}$$

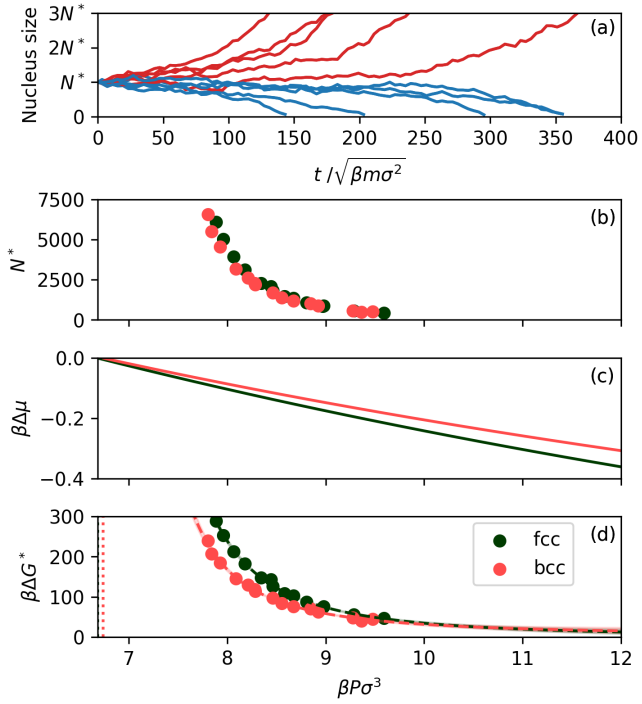

FIG. 2. (a) Largest cluster size of a bcc seed with an initial size $N^* = 2300$ as a function of time $t/\sqrt{\beta m\sigma^2}$ using the seeding technique in 10 independent simulations of charged colloids at a screening length $1/\kappa\sigma = 0.2$. (b) The critical nucleus size N^* of bcc and fcc, (c) supersaturation $\beta\Delta\mu = \beta(\mu_x - \mu_f)$ with μ_x and μ_f the chemical potential of the crystal and fluid phase, respectively, and (d) the Gibbs free-energy barrier $\beta\Delta G^*$, all as a function of pressure $\beta P\sigma^3$.

where N^* is the number of particles of the critical nucleus at the top of the Gibbs free-energy barrier. In the seeding approach, we insert a seed of the crystal structure of interest, either bcc or fcc, in a metastable fluid phase. After carefully equilibrating the crystal seed and its interface with the fluid, we simulate the system for a range of pressures to determine at which pressure, i.e., the critical pressure P^*, the seed will grow or melt with equal probability, while the crystalline seeds will predominately melt for $P < P^*$, and grow for $P > P^*$. In Fig. 2(a), we exemplarily show that a bcc seed of size $N^* \simeq 2300$ melts or grows with 50% probability at a critical pressure $\beta P^*\sigma^3 \approx 8.28$. Subsequently, we obtain the nucleation barrier ΔG^* for this critical nucleus size N^* using Eq. (1) with $|\Delta\mu|$ the supersaturation at this critical pressure P^*. Using fcc and bcc seeds of many different sizes, the seeding approach enables us to determine the nucleation barriers ΔG^* of both crystal polymorphs for supersaturations $|\Delta\mu|$ close to bulk coexistence. Using classical nucleation theory, these nucleation barriers can be fitted and extrapolated to the entire metastable fluid region (see Fig. 2(d) and SM [21]).

We present our seeding simulation results in a kinetic phase diagram in Fig. 3. The kinetic phase diagram shows a region denoted by red where bcc has a lower nucleation barrier than fcc, and a green region, where fcc has a lower nucleation barrier than bcc. For sufficiently high pressures (marked with triangles) the nucleation barriers of fcc and bcc become indistinguishable within our statistical accuracy. Interestingly, there is a region near the triple point where bcc has a lower nucleation barrier than fcc even though it is metastable. This marked result can be explained by a lower interfacial free energy of the fluid with bcc compared to that with fcc, and is thus a manifestation of Ostwald's step rule and Alexander and McTague's conjecture. On the other hand, in a large region near the fluid-fcc binodal, the stable fcc phase has a lower nucleation barrier than the metastable bcc phase. Therefore, in this region both Ostwald's step rule and Alexander and McTague's conjecture are violated.

Finally, we turn our attention to the crystal growth regime. We select the seeding simulations that resulted in crystal growth, and use only simulations with pressures P close to the critical pressure ($\beta|P - P^*|\sigma^3 < 0.2$). We determine the structural composition of the resulting crystals using polyhedral template matching [34]. For low supersaturations, i.e., for pressures close to bulk coexistence, relatively pure crystals are observed. More precisely, we observe that seeds with the crystal structure corresponding to the lowest nucleation barrier retain their initial crystal structure during growth. Notably, bcc seeds in the metastable bcc region grow out to pure bcc crystals as shown in Fig. 3(b), demonstrating that a proper metastable bcc phase forms in this region. For high screening $1/\kappa\sigma < 0.15$ and low supersaturations, fcc seeds grow out into a mixture of fcc and hcp due to stacking faults as shown in Fig. 3(d). On the other hand, there is a large region at higher supersaturation, where fcc and bcc seeds grow out into a polycrystalline mixture of fcc, hcp, and bcc grains. Interestingly, this region corresponds exactly to the region where the nucleation barriers as determined from the seeding approach become indistinguishable (see SM [21]). Additionally, we find that in this region, the fraction of bcc increases with pressure and $1/\kappa\sigma$.

To test our predictions from the seeding simulations, we also perform brute-force crystallization simulations. We again find in agreement with the seeding simulations that the resulting crystals consist of a mixture of fcc, hcp, and bcc grains as determined by polyhedral template matching. To quantify this further, we determine the composition of the crystals by counting the number of fcc, hcp, and bcc particles in the observed nuclei. In Fig. 4, we plot the probability to observe a crystal cluster consisting of N_{bcc} and $N_{\mathrm{fcc}} + N_{\mathrm{hcp}}$ particles in a two-dimensional histogram. Figure 4 clearly shows that the structure of spontaneously formed nuclei are dominated by fcc and hcp in both the nucleation and growth regime, but there are also bcc grains present, even in very large nuclei. As an example, Fig. 3(c) shows a cross section of a spontaneously formed crystal at a

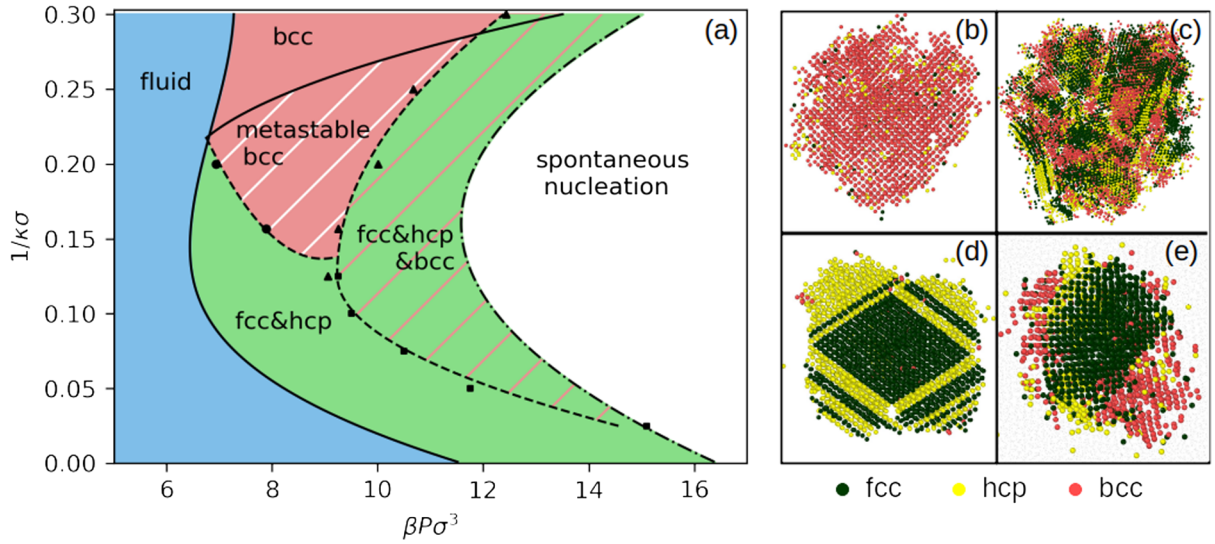

FIG. 3. (a) Kinetic phase diagram of highly charged colloids with a contact value $\beta\epsilon = 81$ in the pressure $\beta P\sigma^3$-Debye screening length $1/\kappa\sigma$ plane. The fluid-fcc, fluid-bcc, and bcc-fcc binodals are denoted by solid lines, and the dash-dotted line marks the pressure beyond which the fluid spontaneously crystallizes. The red (green) region denotes the region where bcc (fcc) has a lower nucleation barrier than fcc (bcc). The red region with stripes near the triple point denotes the metastable bcc region, where bcc has a lower nucleation barrier while being metastable. The triangles mark the pressures above which the nucleation barriers of fcc and bcc are indistinguishable within our statistical accuracy, while the squares mark the pressures above which a mix of fcc, hcp, and bcc is observed in the growth of crystal seeds. The dashed line is a spline interpolation of the triangles and squares, and therefore indicates the onset of a mixed fcc-hcp-bcc region (green with red stripes). Dots are actual measurements and lines are spline interpolations to guide the eye. (b)–(e) Cross sections of crystal nuclei illustrating the different regions in the kinetic phase diagram. The color coding shown below the snapshots denotes the local structure as recognized by the polyhedral template matching, while unrecognized particles are reduced in size. (b) A pure bcc crystal grown from a bcc seed at $(\beta P\sigma^3, 1/\kappa\sigma) = (8.2, 0.2)$; (c) a mix of fcc, hcp, and bcc grains formed spontaneously at $(\beta P\sigma^3, 1/\kappa\sigma) = (11, 0.157)$; (d) a mix of fcc and hcp grown from an fcc seed at $(\beta P\sigma^3, 1/\kappa\sigma) = (8.2, 0.1)$; and (e) a mix of fcc, hcp, and bcc grown from an fcc seed at $(\beta P\sigma^3, 1/\kappa\sigma) = (8.6, 0.157)$.

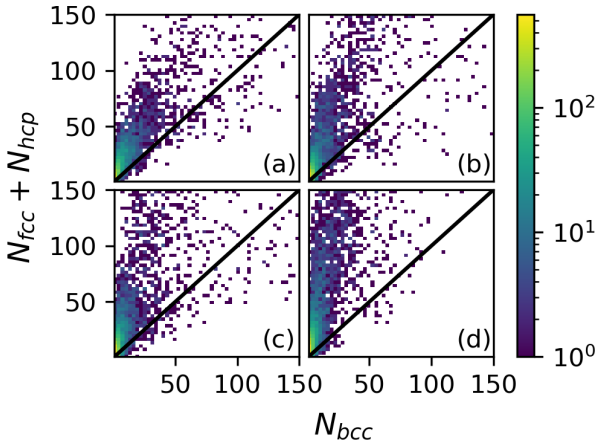

FIG. 4. Two-dimensional histogram of the structure of spontaneously formed crystal nuclei as recognized by polyhedral template matching [34] for varying screening lengths and pressures $(1/\kappa\sigma, \beta P\sigma^3) = (0.3, 15.5)$ (a), (0.2, 12.5) (b), (0.157, 11.5) (c), and (0.1,12.0) (d) as a function of the number of fcc and hcp particles, $N_{\mathrm{fcc}} + N_{\mathrm{hcp}}$, and bcc particles N_{bcc}. The black diagonal line corresponds to $N_{\mathrm{fcc}} + N_{\mathrm{hcp}} = N_{\mathrm{bcc}}$, distinguishing whether crystal nuclei are dominated by fcc and hcp or by bcc.

pressure $\beta P\sigma^3 = 11$ and screening length $1/\kappa\sigma = 0.157$. This nucleus of approximately 10^5 particles clearly shows a combination of fcc, hcp, and bcc crystal grains. We also observe from Fig. 4 that the fraction of bcc increases upon increasing $1/\kappa\sigma$, supporting our earlier findings from seeding simulations.

In conclusion, we summarized our results on crystal polymorph selection in nucleation and growth in a kinetic phase diagram for charged colloids. Our findings as obtained from extensive seeding and brute-force simulations reflect the diversity of previously observed crystallization phenomena in charged colloidal suspensions. For sufficiently low supersaturations, relatively pure crystals are observed, ranging from fcc and hcp to metastable bcc to bcc, upon increasing $1/\kappa\sigma$. The formation of pure metastable bcc phases are in agreement with earlier observations from simulations and experiments [9,10,12,14,15].

For higher supersaturations, we find a mix of fcc, hcp, and bcc crystal grains in a broad region of the phase diagram, in contrast to the predictions of a narrow fcc-bcc coexistence from free-energy calculations [6]. Our findings of a mix of fcc, hcp, and bcc may explain the experimentally observed broad fcc-bcc coexistence region [4,5],

which may be considered as a nonequilibrium state arising by the nucleation and crystallization kinetics. Although fcc and hcp dominate here, the fraction of bcc increases with pressure and screening length.

Comparing our results with Ostwald's step rule or Alexander and McTague's conjecture demonstrates that these crystallization phenomena cannot be captured by simple rules of thumb. By combining our results on the nucleation barriers, spontaneous crystallization, and seeded crystal growth, we obtain a consistent and coherent picture of the different crystallization scenarios for charged colloids. Moreover, our approach is generally applicable and provides a suitable method to effectively predict polymorph selection in future nucleation studies, e.g., oppositely charged colloids [32,35].

M. D. and W. G. acknowledge funding from the European Research Council (ERC) under the European Union's Horizon 2020 research and innovation program (Grant Agreement No. ERC-2019-ADG 884902 SoftML).

*Corresponding author.
w.h.gispen2@uu.nl
†Corresponding author.
m.dijkstra@uu.nl

[1] T. Palberg, Crystallization kinetics of colloidal model suspensions: recent achievements and new perspectives, J. Phys. Condens. Matter **26**, 333101 (2014).
[2] D. M. Herlach, T. Palberg, I. Klassen, S. Klein, and R. Kobold, Overview: Experimental studies of crystal nucleation: Metals and colloids, J. Chem. Phys. **145**, 211703 (2016).
[3] P. Wette and H. J. Schöpe, Nucleation kinetics in deionized charged colloidal model systems: A quantitative study by means of classical nucleation theory, Phys. Rev. E **75**, 051405 (2007).
[4] H. J. Schöpe, T. Decker, and T. Palberg, Response of the elastic properties of colloidal crystals to phase transitions and morphological changes, J. Chem. Phys. **109**, 10068 (1998).
[5] G. Bareigts, P.-C. Kiatkirakajorn, J. Li, R. Botet, M. Sztucki, B. Cabane, L. Goehring, and C. Labbez, Packing Polydisperse Colloids into Crystals: When Charge-Dispersity Matters, Phys. Rev. Lett. **124**, 058003 (2020).
[6] A.-P. Hynninen and M. Dijkstra, Phase diagrams of hard-core repulsive Yukawa particles, Phys. Rev. E **68**, 021407 (2003).
[7] J. K. G. Dhont, C. Smits, and H. N. W. Lekkerkerker, A time resolved static light scattering study on nucleation and crystallization in a colloidal system, J. Colloid Interface Sci. **152**, 386 (1992).
[8] U. Gasser, E. R. Weeks, A. Schofield, P. N. Pusey, and D. A. Weitz, Real-space imaging of nucleation and growth in colloidal crystallization, Science **292**, 258 (2001).
[9] S. Xu, H. Zhou, Z. Sun, and J. Xie, Formation of an fcc phase through a bcc metastable state in crystallization of charged colloidal particles, Phys. Rev. E **82**, 010401(R) (2010).
[10] H. Zhou, S. Xu, Z. Sun, X. Du, and L. Liu, Kinetics study of crystallization with the disorder–bcc–fcc phase transition of charged colloidal dispersions, Langmuir **27**, 7439 (2011).
[11] P. Tan, N. Xu, and L. Xu, Visualizing kinetic pathways of homogeneous nucleation in colloidal crystallization, Nat. Phys. **10**, 73 (2014).
[12] S. Auer and D. Frenkel, Crystallization of weakly charged colloidal spheres: A numerical study, J. Phys. Condens. Matter **14**, 7667 (2002).
[13] R. Blaak, S. Auer, D. Frenkel, and H. Löwen, Crystal Nucleation of Colloidal Suspensions under Shear, Phys. Rev. Lett. **93**, 068303 (2004).
[14] K. Kratzer and A. Arnold, Two-stage crystallization of charged colloids under low supersaturation conditions , Soft Matter **11**, 2174 (2015).
[15] X. Ji, Z. Sun, W. Ouyang, and S. Xu, Crystal nucleation and metastable bcc phase in charged colloids: A molecular dynamics study, J. Chem. Phys. **148**, 174904 (2018).
[16] C. Desgranges and J. Delhommelle, Polymorph selection during the crystallization of Yukawa systems, J. Chem. Phys. **126**, 054501 (2007).
[17] S. Alexander and J. McTague, Should All Crystals Be bcc? Landau Theory of Solidification and Crystal Nucleation, Phys. Rev. Lett. **41**, 702 (1978).
[18] L. O. Hedges and S. Whitelam, Limit of validity of Ostwald's rule of stages in a statistical mechanical model of crystallization, J. Chem. Phys. **135**, 164902 (2011).
[19] J. R. Espinosa, C. Vega, C. Valeriani, and E. Sanz, Seeding approach to crystal nucleation, J. Chem. Phys. **144**, 034501 (2016).
[20] J. Jover, A. J. Haslam, A. Galindo, G. Jackson, and E. A. Müller, Pseudo hard-sphere potential for use in continuous molecular-dynamics simulation of spherical and chain molecules, J. Chem. Phys. **137**, 144505 (2012).
[21] See Supplemental Material at http://link.aps.org/supplemental/10.1103/PhysRevLett.129.098002 for the code, details on molecular dynamics simulations, seeding simulations, and free energy calculations, as well as phase diagrams in the packing fraction-Debye screening length plane, which includes Refs. [22–29].
[22] S. Plimpton, Fast parallel algorithms for short-range molecular dynamics, J. Comput. Phys. **117**, 1 (1995).
[23] B. Widom, Some Topics in the Theory of Fluids, J. Chem. Phys. **39**, 2808 (1963).
[24] R. Freitas, M. Asta, and M. de Koning, Nonequilibrium free-energy calculation of solids using LAMMPS, Comput. Mater. Sci. **112**, 333 (2016).
[25] P. J. Steinhardt, D. R. Nelson, and M. Ronchetti, Bond-orientational order in liquids and glasses, Phys. Rev. B **28**, 784 (1983).
[26] W. Lechner and C. Dellago, Accurate determination of crystal structures based on averaged local bond order parameters, J. Chem. Phys. **129**, 114707 (2008).
[27] J. A. van Meel, L. Filion, C. Valeriani, and D. Frenkel, A parameter-free, solid-angle based, nearest-neighbor algorithm, J. Chem. Phys. **136**, 234107 (2012).

[28] B. Settles, *Active Learning Literature Survey*, Computer Sciences Technical Report 1648 (University of Wisconsin, Madison, 2009).

[29] P. H. Richter, Estimating errors in least-squares fitting, Telecommun. Data Acquis. Prog. Rep. **122**, 107 (1995).

[30] B. Sadigh, L. Zepeda-Ruiz, and J. L. Belof, Metastable–solid phase diagrams derived from polymorphic solidification kinetics, Proc. Natl. Acad. Sci. U.S.A. **118**, e2017809118 (2021).

[31] I. Sanchez-Burgos, E. Sanz, C. Vega, and J. R. Espinosa, Fcc vs. hcp competition in colloidal hard-sphere nucleation: on their relative stability, interfacial free energy and nucleation rate, Phys. Chem. Chem. Phys. **23**, 19611 (2021).

[32] I. Sanchez-Burgos, A. Garaizar, C. Vega, E. Sanz, and J. R. Espinosa, Parasitic crystallization of colloidal electrolytes: growing a metastable crystal from the nucleus of a stable phase , Soft Matter **17**, 489 (2021).

[33] J. R. Espinosa, C. Vega, C. Valeriani, and E. Sanz, The crystal-fluid interfacial free energy and nucleation rate of NaCl from different simulation methods, J. Chem. Phys. **142**, 194709 (2015).

[34] P. M. Larsen, S. Schmidt, and J. Schiøtz, Robust structural identification via polyhedral template matching, Model. Simul. Mater. Sci. Eng. **24**, 055007 (2016).

[35] E. Sanz, C. Valeriani, D. Frenkel, and M. Dijkstra, Evidence for Out-of-Equilibrium Crystal Nucleation in Suspensions of Oppositely Charged Colloids, Phys. Rev. Lett. **99**, 055501 (2007).